Electronic Research Archive

ERA, 31(8): 4882–4906.
DOI: 10.3934/era.2023250
Received: 16 May 2023
Revised: 14 June 2023
Accepted: 29 June 2023
Published: 11 July 2023

http://www.aimspress.com/journal/ERA

*Research article*

# Application of Improved Jellyfish Search algorithm in Rotate Vector reducer fault diagnosis

**Xiaoyan Wu [1], Guowen Ye[2], Yongming Liu[3,4,*], Zhuanzhe Zhao[3,4,*], Zhibo Liu[3] and Yu Chen[1]**

[1] School of Mechanical Engineering, Anhui Polytechnic University, Wuhu 241000, China
[2] Chery New Energy Automotive Co., Ltd, Wuhu 241002, China
[3] School of Artificial Intelligence, Anhui Polytechnic University, Wuhu 241000, China
[4] Anhui Provincial Key Laboratory of Discipline Co-construction on Intelligent Equipment Quality and Reliability, Wuhu 241000, China

* **Correspondence:** Email: liuym@ahpu.edu.cn, zhuanzhe727@ahpu.edu.cn.

**Abstract:** In order to overcome the low accuracy of traditional Extreme Learning Machine (ELM) network in the performance evaluation of Rotate Vector (RV) reducer, a pattern recognition model of ELM based on Ensemble Empirical Mode Decomposition (EEMD) fusion and Improved artificial Jellyfish Search (IJS) algorithm was proposed for RV reducer fault diagnosis. Firstly, it is theoretically proved that the torque transmission of RV reducer has periodicity during normal operation. The characteristics of data periodicity can be effectively reflected by using the test signal periodicity characteristics of rotating machinery and EEMD. Secondly, the Logistic chaotic mapping of population initialization in JS algorithm is replaced by tent mapping. At the same time, the competition mechanism is introduced to form a new IJS. The simulation results of standard test function show that the new algorithm has the characteristics of faster convergence and higher accuracy. The new algorithm was used to optimize the input layer weight of the ELM, and the pattern recognition model of IJS-ELM was established. The model performance was tested by XJTU-SY bearing experimental data set of Xi'an Jiaotong University. The results show that the new model is superior to JS-ELM and ELM in multi-classification performance. Finally, the new model is applied to the fault diagnosis of RV reducer. The results show that the proposed EEMD-IJS-ELM fault diagnosis model has higher accuracy and stability than other models.

**Keywords:** Rotate Vector (RV) reducer; Improved artificial Jellyfish Search (IJS); Extreme Learning

Machine (ELM); Ensemble Empirical Mode Decomposition (EEMD); fault diagnosis

## 1. Introduction

With the rapid development of society and economy and the proposal and implementation of science and technology strategies in the world, the robotics industry has been developing rapidly. Nowadays, robots have been widely used in various production and living fields such as high-end equipment, precision machine tools, aerospace and medical instruments. As one of the very important parts of robots, the high precision Rotate Vector (RV) reducer has the advantages of low noise, compact structure, strong bearing capacity and high transmission efficiency. As the structure of the robot is more and more complex, the correlation between the components is more and more close, especially the key component RV reducer, once failure, it is very likely to lead to a chain reaction, leading to significant economic losses and even casualties. Therefore, it is the key technology to ensure the safe and reliable operation of the equipment to monitor the status of the RV reducer, accurately judge the state of the mechanical operation, timely detect the early failure, and thus carry on the fault diagnosis.

At present, many scholars at home and abroad have begun to study the RV reducer fault diagnosis. Shin et al. [1] and others introduced the development of a life test bench for strain wave retarder for robot precision gear retarder to achieve fault diagnosis and fault prediction. An et al. [2] proposed an Acoustic Emission (AE) measurement of RV reducer fault detection based on Hidden Markov Model (HMM). Chen et al. [3] and others proposed a new method of RV reducer fault diagnosis based on nonlinear output frequency response function and deep convolutional neural network. Rohan et al. [4] proposed an embedded current signal as a method for detecting and diagnosing RV reducer faults. Wang et al. [5] and others realized rapid diagnosis of RV reducer defect parts by using the stiffness fluctuation mechanism of RV reducer, which has strong engineering application value. Raouf et al. [6] and others introduced a novel approach to use the embedded electrical current system for the fault detection of the RV reducer. Xu et al. [7] proposed a compound fault identification method based on improved convolutional capsule network. The above studies promote the development of RV reducer fault diagnosis, but the research methods are more complex, and need a lot of test data support, but often RV reducer in the initial failure of the data characteristics, and most of the fault diagnosis features are from the time domain and frequency domain, while the selection of rotation cycle for fault characteristics is less common.

With the popularization of Internet technology and the development of society, neural network has attracted more and more attention from all walks of life, among which fault diagnosis is one of the fields in which neural network is widely used. Relevant researchers have done a lot of research here [8–10]. Huang et al. [11] and others proposed a deep residual networks-based intelligent fault diagnosis (IFD) method of planetary gearboxes in cloud environments. He and Ye [12] proposed a new bearing fault diagnosis method based on wavelet packet transform and CNN optimized by simulated annealing algorithm. An and Wang [13] proposed a new rolling bearing fault diagnosis algorithm based on overlapping group sparse model—deep complex CNN. Sharma et al. [14] and others proposed a fault diagnosis method based on intelligent non-invasive thermal images, which is used to regularly monitor the condition of rolling contact bearings, so as to understand the deterioration caused by defects of inner ring, outer ring and ball/roller. Wang et al. [15] and others

adopted the ELM method to classify faults of fuel system. Liu and Wang [16] and others proposed a fault prediction method of switch machine based on wavelet energy spectrum entropy and improved extreme learning machine. However, the uncertainty selection of the input weight of traditional ELM will have a great impact on the accuracy of the predicted output results. Now there are a variety of improvement methods, one of which is to optimize the network weight of ELM using optimization algorithms. For example, Ge and Zhang [17] targeted at the influence of the random selection of the input weight of traditional ELM and the threshold of the hidden layer on the classification effect. Adaptive differential evolution extreme learning machine was used to optimize it, so as to ensure fault diagnosis performance. Rayi et al. [18] proposed an efficient hybrid time series prediction model combining variational mode decomposition (VMD) and deep learning hybrid kernel ELM (MKELM) autoencoder (AE). The above scholars have made great contributions in the field of equipment fault diagnosis by using neural networks. In recent years, various fault diagnosis methods based on extreme learning machine have emerged in an endless series, but most of them lack universality, and their prediction results are easily affected by the randomness of ELM weight and threshold value.

Artificial Jellyfish Search (JS) algorithm is a new swarm intelligence algorithm proposed by scholars Chou and Truong [19], who simulated the characteristics of jellyfish fluttering with ocean currents and the internal movement of jellyfish groups. This algorithm has the characteristics of strong optimization searching ability and fast convergence speed. Based on this, in order to overcome the low accuracy of traditional extreme learning machine network in RV reducer performance evaluation, an IJS-ELM fault diagnosis and classification model for industrial robot RV reducer based on EEMD was proposed in this paper. Firstly, EEMD decomposition was performed on the data measured by the RV reducer test platform to obtain several intrinsic mode components (IMF). Secondly, multiple groups of characteristic values were obtained after the overall average checking and optimization of each IMF. Finally, the eigenvalues are imported as input into the Extreme Learning Machine (ELM) optimized by the improved artificial Jellyfish Search algorithm (IJS) for fault diagnosis and comparative analysis of the results. The main contributions include the following:

1) The experimental data of RV reducer were denoised by EEMD, and several sets of eigenvalues were obtained. The eigenvalues were imported into the ELM optimized by the IJS as input, fault diagnosis was carried out, and the results were compared with those of other models.

2) The IJS-ELM fault diagnosis and classification model of RV reducer based on EEMD presented in this paper has high fault recognition rate and stability, and overcomes the problem that the traditional ELM network has low accuracy in the performance evaluation of RV reducer. It can effectively help factories and enterprises reduce losses, and can also help RV reducer test manufacturers to improve the accuracy of measuring RV reducer test data to a certain extent, so as to reduce the economic loss of RV reducer manufacturers and improve the efficiency of RV reducer manufacturers.

The remainder of this paper is structured as follows. Section 2 analyzes the failure modes of industrial robot RV reducers. Section 3 introduces the principles behind the IJS algorithm. Section 4 presents the methodology for constructing an industrial robot RV reducer fault diagnosis and classification model based on EEMD-IJS-ELM. Section 5 describes the experimental procedure and analysis of results, and Section 6 concludes the paper.

## 2. Analysis of failure mode of RV reducer for industrial robots

The structure of RV reducer is planetary wheel structure, as shown in Figure 1 [20]. It consists of a middle solar wheel and two planetary wheels, and its deceleration mechanism is second-order deceleration. The rotation of the input shaft is transmitted to the planet wheel through the center wheel, and the deceleration is carried out according to the tooth ratio. This is the first-stage deceleration. The crankshaft rotates once a week, then the cycloid wheel will rotate a tooth in the opposite direction of the crankshaft, which is a two-stage deceleration.

The fault types of RV reducer are divided into four categories: rolling bearing fault, RV gear fracture fault, crankshaft wear fault and vibration and noise fault [19]. Bearing fault will cause the output torque of RV reducer to rise suddenly and the operation will stop in the short run. The RV wheel impact fault is the RV reducer in mutual meshing load gear pair, the root is subjected to the maximum alternating stress, when the stress exceeds the fatigue limit of the gear material itself, the initial crack appears at the root of the tooth, and continues to extend, when the rest of the parts can't bear the transmission load, it will cause the RV gear broken tooth failure, and directly lead to the RV reducer can't operate. Crankshaft wear usually due to the lack of lubricating oil or poor cleanliness, will lead to wear between the crankshaft and needle bearing, resulting in crankshaft deformation, clearance increase, early failure is not easy to detect, serious fault will lead to a significant increase in transmission efficiency, reduction ratio, RV reducer output power rise, output torque decline. Vibration and noise fault is mainly due to the lack of grease. In the transmission process, mutual collision and friction arouse the vibration of the gear body, and the sound of radiation. Because rolling bearing fault, RV tooth fracture fault and vibration and noise fault are easy to distinguish, the crankshaft wear fault which is not easily detected is selected for research.

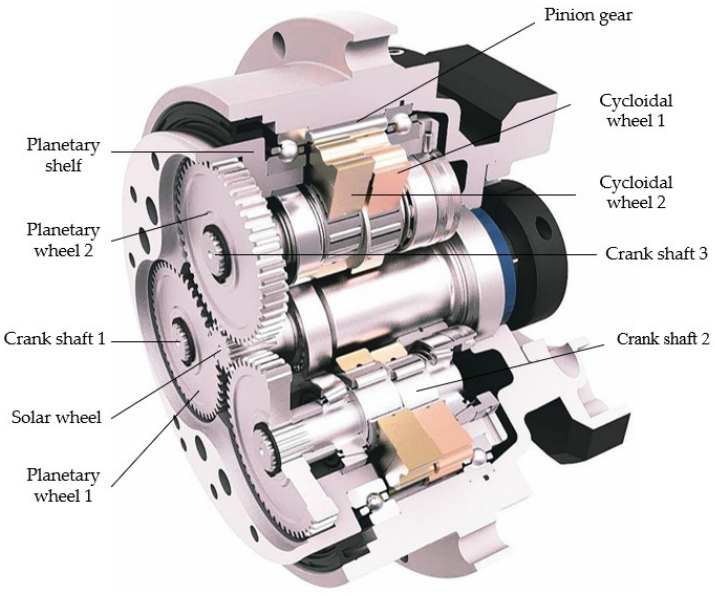


**Figure 1.** Structure diagram of RV reducer of industrial robot.

## 3. Principle of artificial Jellyfish Search algorithm

### *3.1. Standard artificial Jellyfish Search algorithm*

Artificial Jellyfish Search (JS) algorithm was proposed by Jui-Sheng Chou in Taiwan in 2020. It is a new meta-heuristic algorithm. As soft creatures, jellyfish are able to appear almost anywhere in the ocean by moving within their colonies and following ocean currents to form jellyfish blooms. Because the distribution of jellyfish food in the ocean is uneven, jellyfish migrate in the direction of the relatively high proportion of food. The algorithm models the above behavior of jellyfish mathematically.

The population initialization of the JS algorithm was created based on Logistic mapping, as shown in Eq (1).

$$X_{i+1} = \eta X_i(1 - X_i),\ 0 \le X_0 \le 1 \tag{1}$$

In formula, $X_0 \neq \{0.0, 0.25, 0.75, 0.5, 1.0\}$, $\eta = 4$.

The calculation formula of ocean current direction (convergence trend of algorithm) is:

$$\overrightarrow{tr} = X^* - \beta \times rand(0,1) \times \mu \tag{2}$$

In formula, $X^*$ is the position of the optimal jellyfish, that is, the optimal parameter value of the optimization model. $\mu$ is the average position of all jellyfish, $\beta = 3$ is the distribution coefficient, and the updated formula of each jellyfish's position is:

$$X_i(t+1) = X_i(t) + rand(0,1) \times (X^* - \beta \times rand(0,1) \times \mu) \tag{3}$$

The optimization motion of jellyfish is mainly divided into passive motion and active motion. The mathematical model of passive motion is shown as follows:

$$X_i(t+1) = X_i(t) + \gamma \times (U_b - L_b) \tag{4}$$

In formula, $U_b$ and $L_b$ are the upper and lower limits of the search space respectively, and $\gamma = 0.1$ is the motion coefficient.

The mathematical model of active motion is shown in Eq (5).

$$X_i(t+1) = X_i(t) + rand(0,1) \times \vec{D} \tag{5}$$

In formula, $\vec{D}$ represents the location of the most food, as shown in Eq (6).

$$\vec{D} = \begin{cases} X_j(t) - X_i(t) & if\ f(X_i) \ge f(X_j) \\ X_i(t) - X_j(t) & if\ f(X_i) < f(X_j) \end{cases} \tag{6}$$

The jellyfish can move passively with ocean currents, or they can move within the colony for subject motion, and the "time control mechanism" controls the transition between these movement types. Time control mechanism includes time control function *c(t)* and constan $C_0 = 0.5$.

$$c(t) = \left|\left(1 - \frac{t}{Max_{iter}}\right) \times (2 \times rand(0,1) - 1)\right| \tag{7}$$

When *c(t)* is greater than $C_0$, jellyfish will actively move. When *c(t)* is less than $C_0$, the jellyfish will move passively.

### *3.2. Improved artificial Jellyfish Search algorithm (IJS)*

The Improved artificial Jellyfish Search algorithm (IJS) mainly uses tent mapping to replace the Logistic chaotic mapping of population initialization in the artificial Jellyfish Search algorithm, and introduces the competition mechanism.

The core formula for tent mapping is shown in Eq (8):

$$x_{n+1} = a - (1 + a)|x_n| \qquad a \in (0,1) \tag{8}$$

The traversal of the tent mapping exhibits uniformity and randomness, enabling the algorithm to easily escape local optima, thereby maintaining population diversity and improving global search capability.

The competitive mechanism is designed to ensure the stability of the tent mapping. After generating an initial solution with the tent mapping, K iterations are performed to select the best initial population.

Based on this, the standard JS algorithm is improved as follows:

Step 1: IJS initialization parameters: search space, population dimension, population size, maximum number of iterations, etc.

Step 2: Population initialization. Initialize the jellyfish population *X, X* is calculated using tent chaotic mapping. At the same time, in order to ensure the stability of tent mapping, K iterations are carried out according to the dimension of initial solution generated by tent mapping to select the optimal initial population. The food at each position is defined by $f(X_i)$.

Step 3: Find the jellyfish that is currently in the best position and set the initialization time t = 1.

Step 4: Calculate the control time *c(t)* when $i = 1$.

Step 5: Let's figure out what *c(t)* is, when $c(t) \geq 0.5$, update the current formula, update the current current, update the current position. When $c(t) < 0.5$, Then, a number between 0 and 1 is randomly generated to see if it is greater than 1- *c(t)*. If it is greater than 1- *c(t)*, the position is updated in the original direction of jellyfish; if it is less than 1- *c(t)*, the equation is needed to determine the direction of jellyfish and continue updating with the new position.

Step 6: Check the boundary conditions and calculate the amount of food in the new location while updating the position to jellyfish *X* and the current best Jellyfish *X**.

Step 7: Repeat steps 1 to 6 of the cycle with the number of cycles equal to the number of initialized populations.

Step 8: Repeat step 1 to Step 7 to determine whether the obtained value reaches the iteration termination condition.

Step 9: The competition mechanism is introduced, the above steps are repeated several times, and the optimal value is selected as the output result.

The main steps of IJS algorithm are shown in Figure 2.

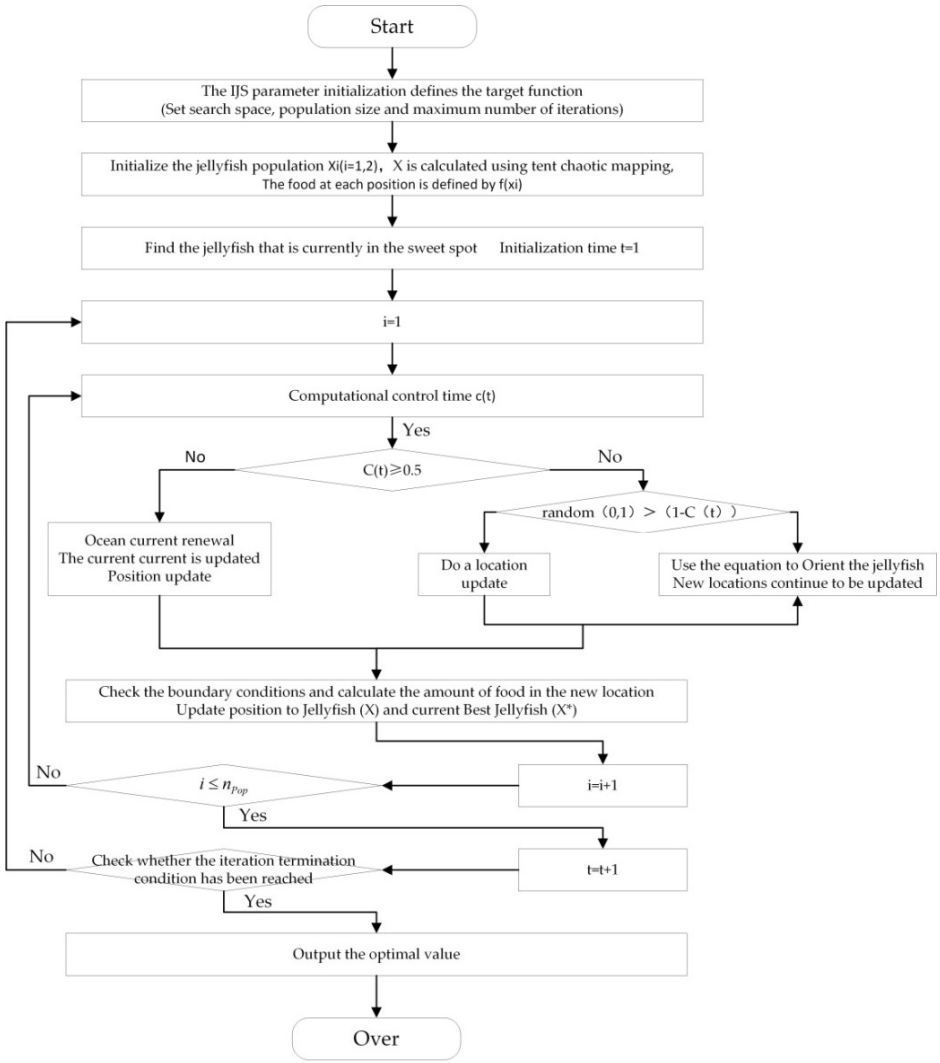


**Figure 2.** IJS algorithm flow diagram.

### *3.3. Performance test of IJS algorithm*

In order to objectively evaluate the performance of IJS algorithm, four test functions [21] widely used for single objective optimization were selected for simulation experiment verification. The experimental environment information is shown in Table 1. Besides, dimension D is set as 15, and its global minimum value is 0. The test function used is shown in Table 2, the test results are shown in Table 3 and Figures 3–6.

**Table 1.** Experimental environment information.

| Type | Parameter |
|---|---|
| Operating environment | MATLAB2020b |
| CPU | lntel(R)Core(TM) i7-9750H CPU @ 2.60GHz |
| Operating system type | 64-bit |
| Memory | 24G |

**Table 2.** Test function information.

| Function name | Expression | Range |
|---|---|---|
| Sphere | $F_1(x) = \sum_{i=1}^{D} x_i^2$ | [-100, 100] |
| Schwefel 1.2 | $F_2(x) = \sum_{i=1}^{D} \left( \sum_{j=1}^{i} x_j \right)^2$ | [-100, 100] |
| Schwefel 2.21 | $F_3(x) = max_i\{\|x_i\|, 1 \le i \le D\}$ | [-100, 100] |
| Griewank | $F_4(x) = \sum_{i=1}^{D} \frac{x_i^2}{4000} - \prod_{i=1}^{D} cos\left(\frac{x_i}{\sqrt{i}}\right) + 1$ | [-600, 600] |

In order to test the performance of IJS and JS Algorithm, standard Particle Swarm Optimization (PSO) and Genetic Algorithm (GA) are added to compare the optimization results. Considering the fairness of the experiment, the common parameters of each algorithm are set uniformly. According to [22], it is assumed that the population number A = 30 and the maximum number of iterations T = 2000. According to the recommended value in [23], inertia weight was set as 0.729 and learning factor as 1.49445 in PSO. According to [24], GA algorithm in this section had crossover probability as 0.5 and mutation probability as 0.01. According to [19], JS algorithm and IJS algorithm had distribution coefficient as 3 and motion coefficient as 0.1.

In order to avoid accidental errors, each algorithm program is run independently for 30 times, and the optimal value, mean value and variance obtained from the results are counted and recorded in Table 3.

**Table 3.** Function test result.

| Function | Algorithm | Optimum value | Mean value | Variance |
|---|---|---|---|---|
| F1 | GA | 1.4415E-13 | 1.8847E-12 | 2.2356E-12 |
| | PSO | 2.0106E-17 | 2.2015E-17 | 8.5528E-19 |
| | JS | 4.0158E-129 | 2.7241E-113 | 8.1698E-113 |
| | IJS | 2.4132E-146 | 6.0147E-135 | 1.4935E-134 |
| F2 | GA | 3.3378E-01 | 2.0468E+00 | 1.9115E+00 |
| | PSO | 1.9293E-17 | 6.4631E-07 | 1.9389E-06 |
| | JS | 2.2467E-17 | 2.0440E-05 | 3.6592E-05 |
| | IJS | 5.9691E-31 | 2.2227E-22 | 6.4602E-22 |
| F3 | GA | 1.6607E-14 | 1.7940E-14 | 9.4270E-16 |
| | PSO | 3.6301E-32 | 1.1548E-29 | 2.0827E-29 |
| | JS | 3.5067E-45 | 5.1454E-40 | 1.4885E-39 |
| | IJS | 2.3063E-80 | 3.6732E-76 | 6.8374E-76 |
| F4 | GA | 5.8028E-02 | 1.4297E+00 | 2.0074E+00 |
| | PSO | 1.9293E-17 | 8.2117E-17 | 1.2565E-16 |
| | JS | 0.0000E+00 | 0.0000E+00 | 0.0000E+00 |
| | IJS | 0.0000E+00 | 0.0000E+00 | 0.0000E+00 |

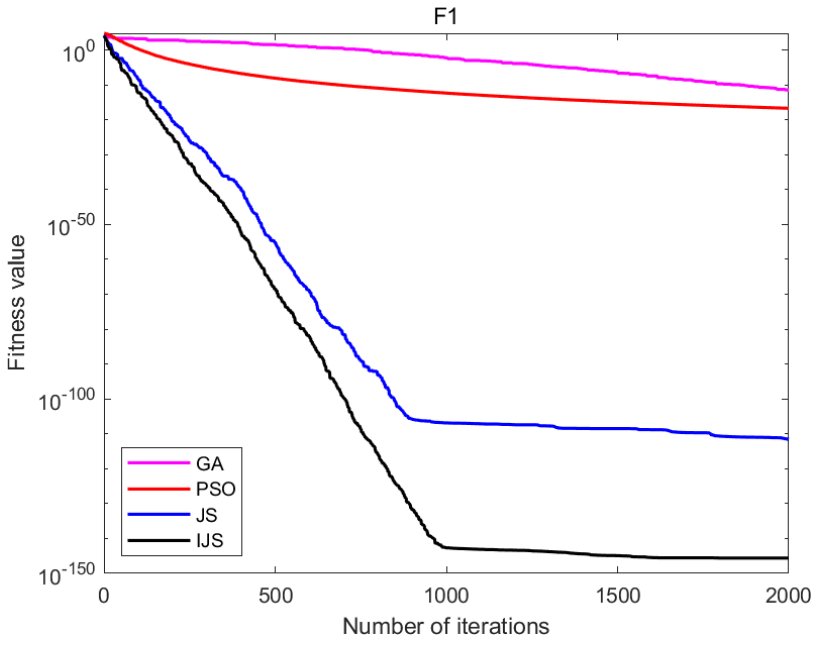


**Figure 3.** Comparison of F1 fitness of GA, PSO, JS and IJS.

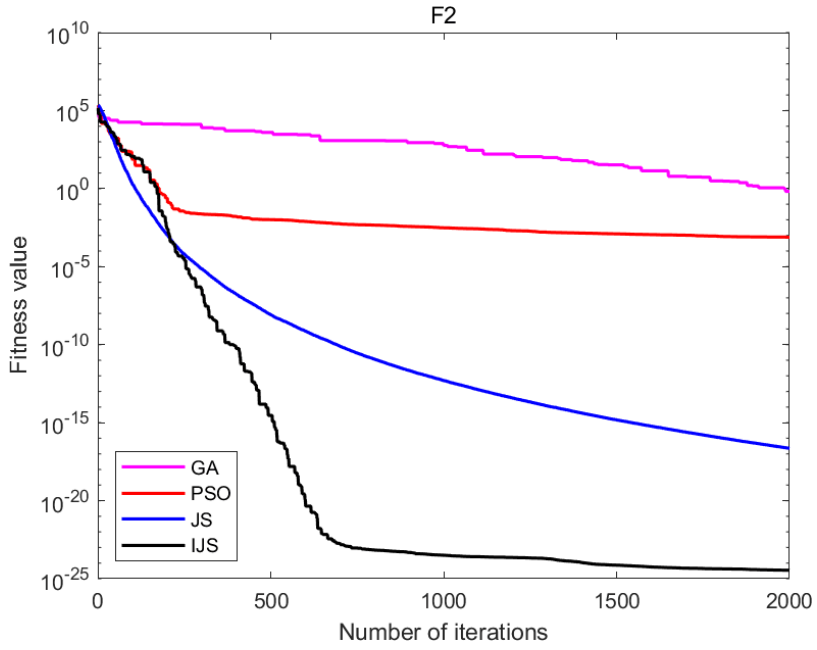


**Figure 4.** Comparison of F2 fitness of GA, PSO, JS and IJS.

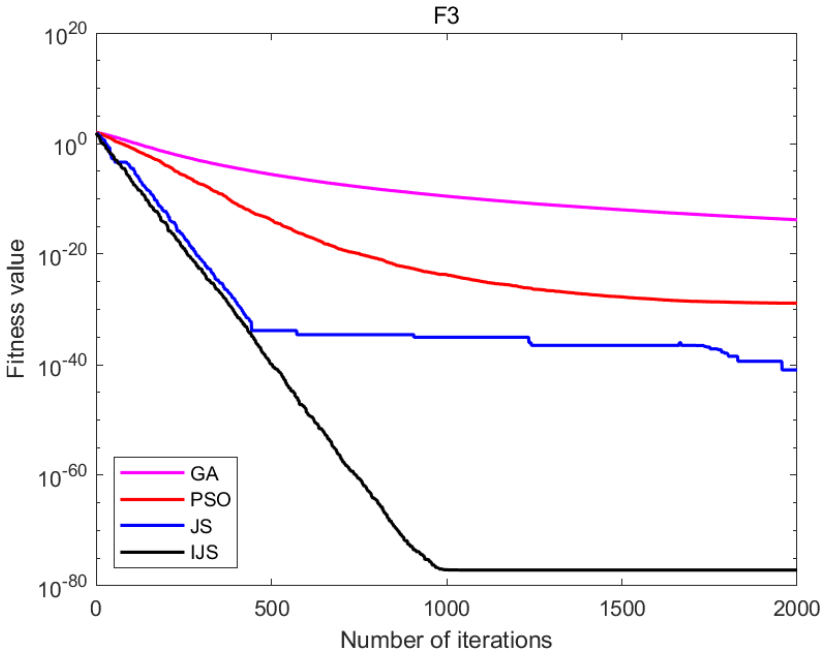


**Figure 5.** Comparison of F3 fitness of GA, PSO, JS and IJS.

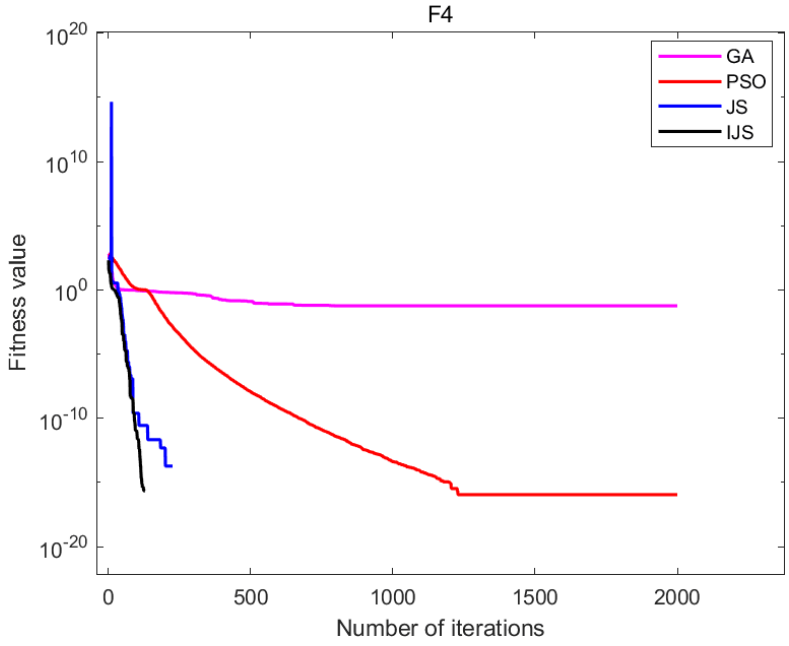


**Figure 6.** Comparison of F4 fitness of GA, PSO, JS and IJS.

It can be seen from Table 3, Figures 3 and 5 that compared with GA, PSO and JS, in test standard function 1 and test standard function 3, IJS is superior to GA, PSO and JS in both solving accuracy and iteration speed. In Figure 4, IJS is equal to PSO and JS in iteration speed and accuracy before 400 times, but after 400 times, The iteration speed and accuracy of IJS are both higher than GA, PSO and JS. After 2000 iterations, the accuracy of IJS is about $10^5$ higher than that of JS. As can be seen from Figure 6, both IJS and JS converge on test function 4, and IJS converges faster. To

some extent, IJS has higher convergence accuracy than JS.

## 4. Establishment of EEMD-IJS-ELM model

### *4.1. EEMD preprocessing*

Using rotating machinery to measure the periodic evolution characteristics of signal and integrated empirical mode decomposition can more effectively and intuitively reflect the periodic change characteristics of data. Empirical Mode Decomposition (EMD) is an adaptive signal analysis method, but there are some problems such as mode aliasing and screening iteration stop criteria. To solve these problems, Wu et al. [25] proposed EEMD. In this method, white noise is added to fill the signal in the discontinuous signal segment, so that the extreme points of the signal are evenly distributed and the mode aliasing phenomenon is overcome [26].

The steps of EEMD preprocessing are as follows [27]:

Step 1: Divide the fault data into several sample data, and add normal white noise $S_w(\omega)$ to each sample data x(t) to obtain a new overall $x_s(t)$.

Step 2: The sample data $x_s(t)$ is decomposed by EMD, and the decomposition results are as follows:

$$x_s(t) = \sum_{c=1}^{n} imf_c(t) + r_n(t) \tag{9}$$

Among them, $imf_c(t)$ represents the c IMF of EEMD decomposition, $r_n(t)$ refers to the residual component after EEMD decomposes n IMFs.

Step 3: Repeat steps 1 and 2 above, adding a new white noise sequence each time.

Step 4: All the IMF received is processed by taking a definite integral and dividing it by the length of the segment.

### *4.2. Establishment of IJS-ELM model*

Extreme Learning Machine (ELM) is an algorithm for Single-hidden Layer Feedforward-Neural Network (SLFN) proposed by Huang [28]. ELM has few training parameters, fast learning speed, powerful and other characteristics. In the training process, the connection weight $W$ and threshold $B$ between the input layer and the hidden layer are generated randomly, and then the connection weight is multiplied and superimposed with the input matrix of the training set. Since $W$ and $B$ is generated randomly, the accuracy of ELM is affected to some extent. The IJS algorithm is used to optimize the ELM weight $W$ and the threshold $B$ of the implicit neuron to improve the accuracy of ELM.

Step 1: Let the connection weight W between the input layer and the hidden layer be:

$$\mathrm{W} = \begin{bmatrix} W_{11} & W_{12} & \cdots & W_{1m} \\ W_{21} & W_{22} & & W_{2m} \\ \vdots & & \ddots & \vdots \\ W_{l1} & W_{l2} & \cdots & W_{lm} \end{bmatrix}_{l \times m} \tag{10}$$

Let the threshold $B$ of the hidden layer neurons be:

$$\mathrm{B} = \begin{bmatrix} B_1 \\ B_2 \\ \vdots \\ B_l \end{bmatrix}_{l\times 1} \tag{11}$$

The velocity and position of $W$ and $B$ as IJS are substituted to obtain the optimal solution.

Step 2: The fitness function was defined, the original weight $W$ and threshold $B$ of ELM were obtained from the particles of IJS, and $n$ randomly different training samples were used to practice the ELM neural network.

$$\sum_{i=1}^{L} \beta_i g_i(x_j) = \sum_{i=1}^{L} \beta_i \, g_i(w_i \cdot x_j + B_i) \tag{12}$$

In the formula, $i = 1,2,3,\ldots,n$, $x_i = [\, x_{i1}, x_{i2}, \ldots, x_{id}]^T \in \mathrm{R}^{\mathrm{d}}$, $t_i = [\, t_{i1}, t_{i2}, \ldots, t_{ik}]^T \in \mathrm{R}^{\mathrm{k}}$, $x_i$ and $t_i$ represent the eigenvalue and the real value of the output of the training sample respectively. $d$ and $k$ represent the dimensions of the input characteristic value and the output true value respectively. $L$ represents the number of hidden layer nodes. $j = 1,2,3,\ldots,n$. $g(x)$ is the excitation function. $\beta_i = [\beta_{i1}, \beta_{i2}, \ldots, \beta_{ik}]$ is the connection weight between the ith node of the hidden layer and the output layer.

Write Eq (12) in matrix form:

$$H \cdot \beta = T \tag{13}$$

In the formula,

$$H = \begin{bmatrix} g_1(W_1 \cdot x_1 + B_1) & \cdots & g_L(W_1 \cdot x_1 + B_1) \\ \vdots & \ddots & \vdots \\ g_1(W_1 \cdot x_n + B_n) & \cdots & g_L(W_1 \cdot x_n + B_n) \end{bmatrix} \tag{14}$$

$$\beta = \begin{bmatrix} \beta_1^T \\ \beta_2^T \\ \vdots \\ \beta_L^T \end{bmatrix} \tag{15}$$

$$T = \begin{bmatrix} t_1^T \\ t_2^T \\ \vdots \\ t_n^T \end{bmatrix} \tag{16}$$

$H$ is the implied output matrix, $T$ is the expected output vector matrix.

Using the least square method to solve $\beta$, we can obtain:

$$\beta = H^{+}T = H^T(HH^T)^{-1}T \tag{17}$$

In Eq (17), $H^{+}$ is the Moore-Penrose generalized inverse matrix of matrix $H$, $E$ is an identity matrix and it has the same dimension as $HH^T$; G is a constant.

Step 3: The fitness value of the particle is measured, and the optimum value of the individual and its global value are obtained by taking the root mean square error as fitness function.

Step 4: If the target error is reached, the optimal weight $W$ and hidden layer threshold $B$ will be obtained. If it is not reached, it will return to the upper layer for further optimization until the

maximum number of iterations.

In summary, the fault diagnosis process of IJS-ELM is shown in Figure 7.

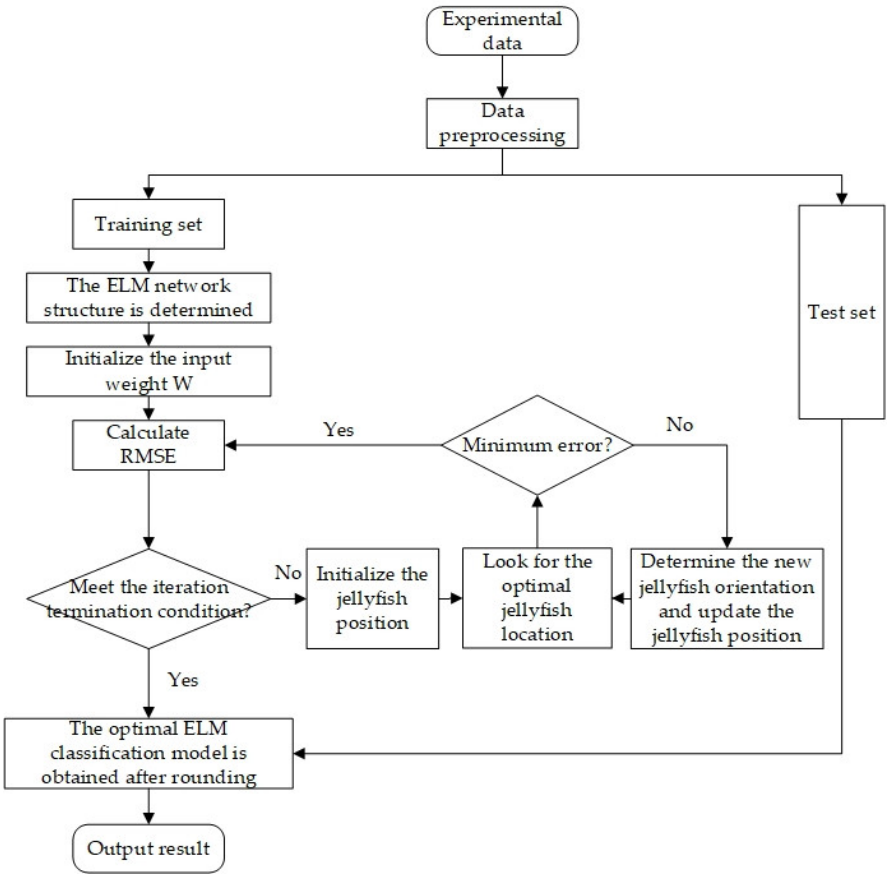


**Figure 7.** IJS-ELM fault diagnosis flow diagram.

### *4.3. Performance test of EEMD-IJS-ELM model*

XJTU-SY bearing experimental data set of Xi'an Jiaotong University was adopted for model test [29]. In the experiment, sampling frequency was set as 25.6 kHz, sampling interval was 1min, and each sampling duration was 1.28 s. The speed of bearings is set at 2100 r/min, and the radial force received is 12 kN. Each sample contains 32,768 sets of data, and each set of data contains one vertical acceleration data and one horizontal acceleration data. It can be seen from [28] that horizontal vibration signals can contain more degradation information, so the standard deviation of horizontal acceleration is selected as the evaluation standard and Bearing1_1, Bearing1_4 and Bearing1_5 in the data set are used as the failure test data set, and the first 10 non-failure samples of Bearing1_4 are selected as the normal data set. The corresponding fault forms are shown in Table 4 and Figure 8.

**Table 4.** Bearing data information.

| Data set group | Number of samples | Actual running time | Failure location |
|---|---|---|---|
| Bearing1_1 | 123 | 2h41min | Outer ring |
| Bearing1_4 | 122 | 2h2min | Cage |
| Bearing1_5 | 52 | 52min | Inner ring, Outer ring |
| Bearing1_4 First 10 samples | 10 | 10min | Normal |

Figure 8(a) shows the failure form of Bearing1_1 dataset, Figure 8(b) shows the failure form of Bearing1_4 dataset, Figure 8(c) shows the failure form of Bearing1_5 dataset, and Figure 8(d) shows the normal form of the first 10 samples of Bearing1_4 dataset.


**Figure 8.** Bearing failure pattern.

Firstly, the total data samples were divided into 16 groups on average. Secondly, EEMD decomposition was carried out on them. Finally, IMF after EEMD decomposition was taken as the input of the proposed model, and the fault classification number was taken as the output. Where 1 means bearing outer ring failure, 2 means cage failure, 3 means inner ring and outer ring failure, 4 means bearing normal. The prediction results of the single EEMD-JS-ELM model are shown in Table 5. The main parameters are set as follows: according to [30], the number of neurons in ELM hidden layer is set as 5, and the activation function is sigmoid. The velocity range of the particle is [-1, 1], the position range is set to [0.3, 0.9], the maximum number of iterations is 100, c1 = 2.8, c2 = 1.3.

**Table 5.** Single model prediction results.

| Sample number | Actual class | ELM | JS-ELM | IJS-ELM |
|---|---|---|---|---|
| 1 | 1 | 1 | 1 | 1 |
| 2 | 2 | 3 | 2 | 2 |
| 3 | 3 | 2 | 3 | 3 |
| 4 | 4 | 4 | 4 | 4 |
| 5 | 1 | 3 | 1 | 1 |
| 6 | 2 | 2 | 1 | 2 |
| 7 | 3 | 1 | 3 | 3 |
| 8 | 4 | 2 | 4 | 4 |
| 9 | 1 | 3 | 1 | 1 |
| 10 | 2 | 2 | 2 | 2 |
| 11 | 3 | 3 | 3 | 3 |
| 12 | 4 | 4 | 4 | 4 |
| 13 | 1 | 1 | 2 | 1 |
| 14 | 2 | 2 | 2 | 2 |
| 15 | 3 | 3 | 3 | 3 |
| 16 | 4 | 3 | 4 | 4 |
| Accuracy rate | | 56.25% | 87.5% | 100% |

According to Table 5, we can know that the single classification accuracy of simple ELM is only 56.25%, and the accuracy of JS-ELM in single operation is 87.5%, which is higher than that of simple ELM model. The accuracy of IJS-ELM in single operation reaches 100%, the highest accuracy among the three models.

To further validate the superior performance of the proposed fault diagnosis model based on EEMD-IJS-ELM and to eliminate experimental randomness, this study compared the performance of this model with seven other models, namely ELM, EEMD-ELM, EEMD-PNN, EEMD-GRNN, EEMD-DE-ELM, EEMD-PSO-ELM, and EEMD-GA-ELM. A total of 20 experiments were conducted, and the prediction results are presented in Figure 9 and Table 6.

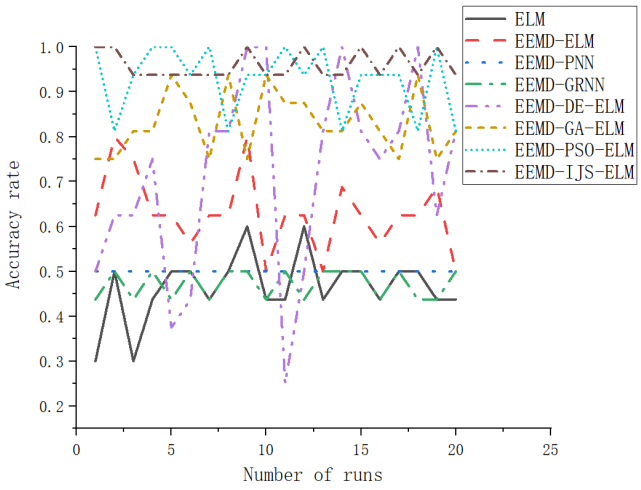


**Figure 9.** Statistics of accuracy of 20 tests of various models.

**Table 6.** Average statistics of recognition accuracy of various models in 20 tests.

| Fault diagnosis model | ELM | EEMD-ELM | EEMD-PNN | EEMD-GRNN | EEMD-DE-ELM | EEMD-GA-ELM | EEMD-PSO-ELM | EEMD-IJS-ELM |
|---|---|---|---|---|---|---|---|---|
| Accuracy rate | 46.5% | 63% | 50% | 47.5% | 71.6% | 83.1% | 92.8% | 95.9% |

Based on Figure 9 and Table 6, it can be observed that the ELM model has the lowest accuracy and is unstable, with accuracy fluctuating between 30 to 60%, and an overall accuracy of only 46.5%. The addition of EEMD to the ELM model significantly improved its accuracy, with an overall accuracy of 63%. However, it remained unstable with fluctuations between 50 to 80%. Although the EEMD-PNN and EEMD-GRNN models were stable, their accuracy was not as high as the EEMD-ELM model, with overall accuracies of only 50 and 47.5%, respectively. This indicates that the accuracy of ELM is higher than that of ordinary neural networks. While the occasional accuracy of the EEMD-DE-ELM model reached 100%, its accuracy was generally low, with a minimum accuracy of only 25%, making it highly unstable. The EEMD-GA-ELM model had a relatively high accuracy, mostly around 80%, occasionally reaching 90%. The EEMD-PSO-ELM model had a high overall accuracy, with an average accuracy of 92.8% over 20 experiments, and an overall accuracy of over 90%, with a few experiments reaching 100%. Its accuracy was relatively stable. The EEMD-IJS-ELM model had the highest accuracy, with an average accuracy of 95.9% over 20 experiments, and the most stable performance, with accuracy fluctuating only between 90 to 100%. Based on these results, it can be concluded that the EEMD-IJS-ELM model is highly suitable for fault diagnosis in RV reducers.

## 5. Experiment and result analysis

### *5.1. Experimental equipment*

The data used in this paper are provided by the RV reducer test platform built in the laboratory. The structure of the test platform is shown in Figure 10. The servo motor has a power of 5 kW, the torque sensor has a range of 200 N·m, the force sensor has a range of 500 N·m, and the magnetic powder brake has a specification of 1.5 kW. The spindle speed is set to 151 r/min, and the data from both the input and output shafts of the RV reducer are measured by the torque sensor. The model of the RV reducer used in the experiment is RV-20E. The data were sampled every 0.5 seconds, and the experiments were conducted at room temperature for a total of 200 hours. The model and parameter specifications of the RV reducer platform are presented in Table 7.

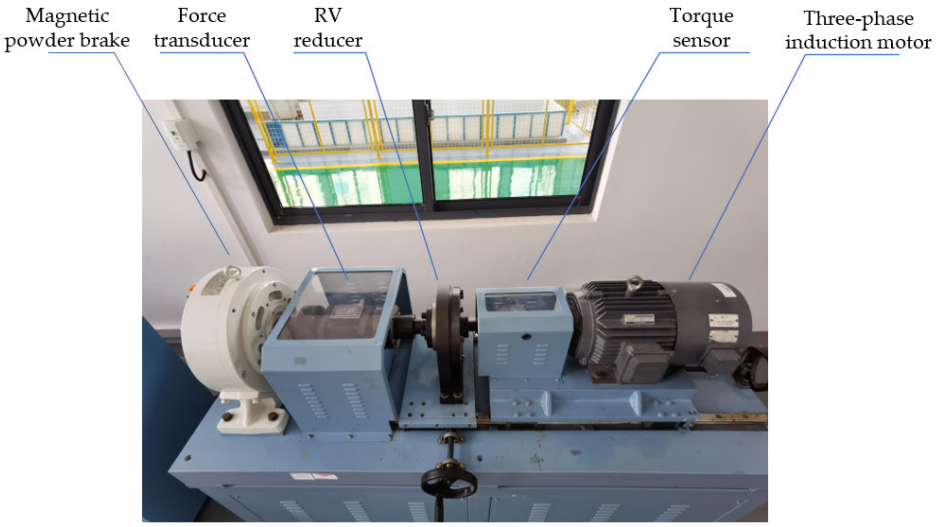


**Figure 10.** RV reducer test platform.

**Table 7.** Type parameters of RV reducer platform.

| Equipment | Model number |
|---|---|
| servomotor | Panasonic MSME502GCG |
| Torque sensor | NCNJ-101(0 ± 15 N·m) |
| RV reducer | RV-20E |
| Torque sensor | NCNJ-101(0 ± 200 N·m) |
| Magnetic powder brake | FZ400A-1 |

During the experiment, abnormal data of torque, speed, and power were observed from the RV reducer, indicating a malfunction. Therefore, data collected prior to the occurrence of the malfunction were selected and compared with efficiency data collected after the malfunction.

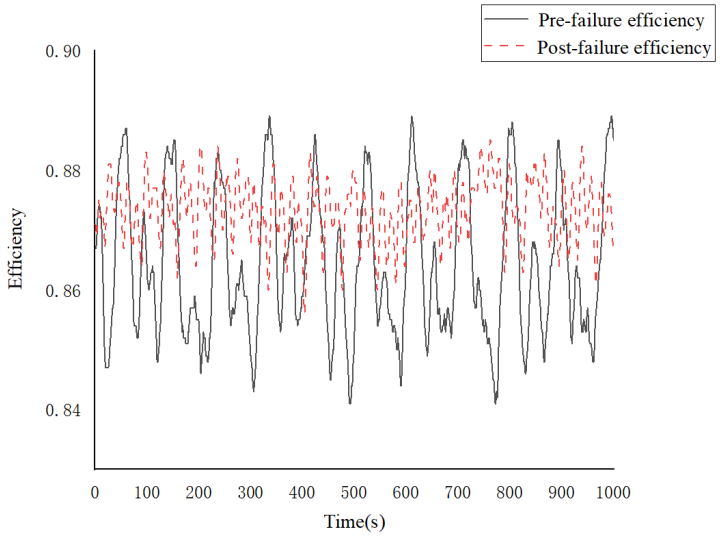


**Figure 11.** Efficiency comparison before and after failure.

According to Figure 11, we can know that the efficiency of RV reducer has a certain periodicity before failure, but the efficiency does not show a periodic change after failure obviously. After disassembling the RV reducer, it was found that the crankshaft was worn, as shown in Figure 12. In order to ensure the transmission stiffness of the test system, a certain preload is applied to the axial connection. The application of the preload and the existence of coaxiality error lead to some partial load in the gear meshing. After the failure, the wear of the RV reducer crank leads to the weak sliding of the planetary wheel along the axis, the preload decreases, the included Angle between the crankshaft force and the axial force decreases, and the radial component of the crankshaft force decreases. The eccentricity h decreases, the gear meshing off-load state and lubrication state improve, and the friction at the meshing point decreases, leading to the increase of transmission efficiency after failure.

**Figure 12.** The crankshaft is worn.

*5.2. Simulation of RV Reducer fault model of EEMD-IJS-ELM*

1680 efficiency data before and after RV reducer failure were selected as sample data, and EEMD decomposition was performed on them, and some graphs were obtained as shown in the figure below.

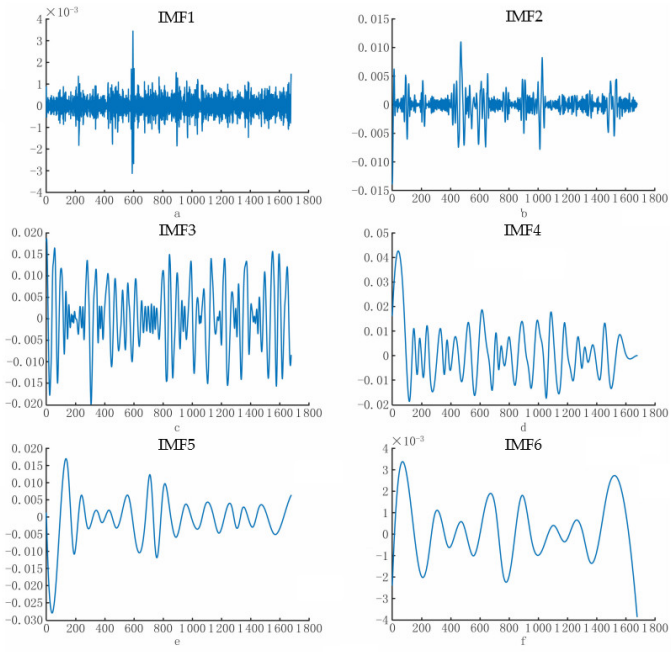


**Figure 13.** Image of normal bearing data after EEMD decomposition. (a) IMF1 component; (b) IMF2 component; (c) IMF3 component; (d) IMF4 component; (e) IMF5 component; (f) IMF6 component (residual component).

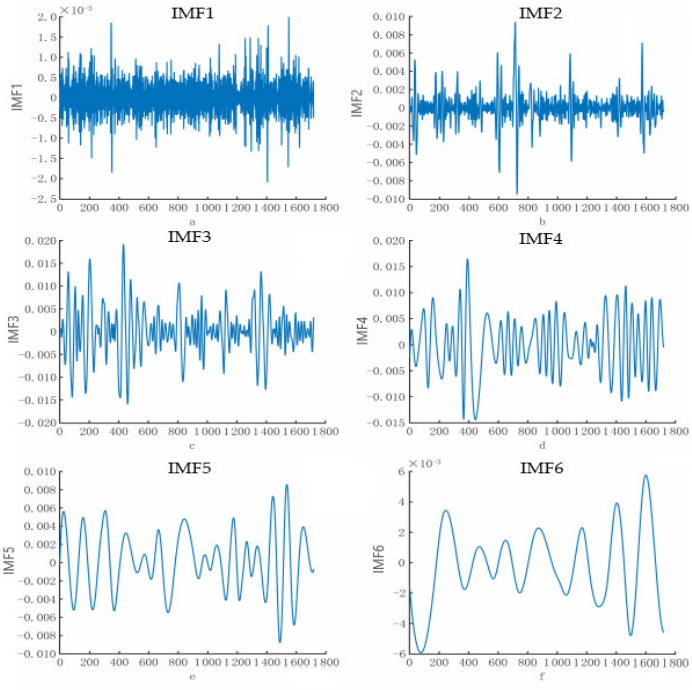


**Figure 14.** Image of fault bearing data after EEMD decomposition. (a) IMF1 component; (b) IMF2 component; (c) IMF3 component; (d) IMF4 component; (e) IMF5 component; (f) IMF6 component (residual component).

According to Figures 13 and 14, we can know that normal data and fault data have obvious

differences after EEMD decomposition. As the energy of the signal is mainly concentrated in the lower IMF components, the first six IMF components were selected for each group and their average value was calculated for verification. After the average calculation of the two groups of data, 21 eigenvalues were obtained respectively, and then the obtained eigenvalues were input into the proposed IJS-ELM fault classification model for training and testing. The results of single operation of the model are shown in Table 8.

**Table 8.** Comparison of single prediction results of RV Reducer fault classification.

| Sample number | Actual class | EEMD-ELM | EEMD-JS-ELM | EEMD-IJS-ELM |
|---|---|---|---|---|
| 1 | 1 | 2 | 1 | 1 |
| 2 | 2 | 2 | 2 | 2 |
| 3 | 1 | 1 | 1 | 1 |
| 4 | 2 | 1 | 1 | 2 |
| 5 | 1 | 2 | 1 | 1 |
| 6 | 2 | 1 | 2 | 2 |
| 7 | 1 | 2 | 1 | 1 |
| 8 | 2 | 2 | 2 | 2 |
| 9 | 1 | 1 | 1 | 1 |
| 10 | 2 | 2 | 1 | 2 |
| Accuracy rate | | 50% | 80% | 100% |

According to Table 8, we can know that the accuracy of IJS-ELM in single fault classification of RV reducer reaches 100%, which is higher than that of simple ELM which is 50%. In order to eliminate the chance of a single experimental result, the universality of the proposed model is confirmed, it was run 20 times in total, and the fault diagnosis accuracy of each model is shown in the Table 8.

According to Table 9, we can know that the accuracy rate of ELM is only 61.5%, and the accuracy rate of JS-ELM is much higher than that of ELM, reaching 86%, while the accuracy rate of IJS-ELM is up to 95%.

**Table 9.** Model accuracy statistics.

| Fault diagnosis model | EEMD-ELM | EEMD-JS-ELM | EEMD-IJS-ELM |
|---|---|---|---|
| Accuracy rate | 61.5% | 86% | 95% |

In order to further verify the performance superiority of the proposed RV reducer fault diagnosis model based on EEMD-IJS-ELM, this paper compares and analyzes the diagnosis results of this model with other models. EEMD-IJS-ELM was compared with seven models, ELM, EEMD-ELM, EEMD-PNN, EEMD-GRNN, EEMD-DE-ELM, EEMD- GA -ELM and EEMD-PSO-ELM, and the results are shown in Figure 15.

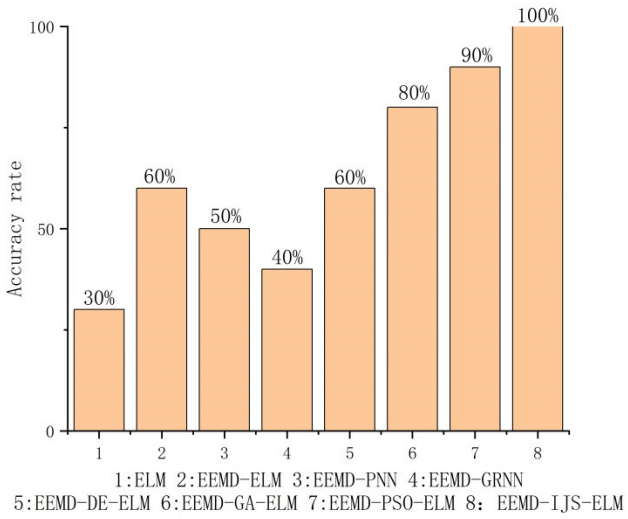


**Figure 15.** Prediction results of single test of multiple models.

According to Figure 15, the identification accuracy of ELM would be as low as 30%, and by adding EEMD, the accuracy would be significantly improved to 60%, and the effect would be significant. Probabilistic Neural Network (PNN) and Generalized Neural Network (GRNN) show poor performance, the accuracy of which is 50 and 40%, respectively. Differential Evolution (DE) algorithm optimizes ELM, however, has poor predictive effect in this experiment. The effect of ELM optimized by Genetic Algorithm (GA) was obvious in this experiment, and the accuracy rate reached 80%. The accuracy of EEMD-PSO-ELM recognition model in the test results reached 90%, meanwhile, the accuracy of EEMD-IJS-ELM in the test results prediction reached 100%.

In order to eliminate the chance of a single experimental result, the universality of the proposed model is confirmed, it was run 20 times in total, and the fault diagnosis accuracy of each model is shown in Figure 16 and Table 10.

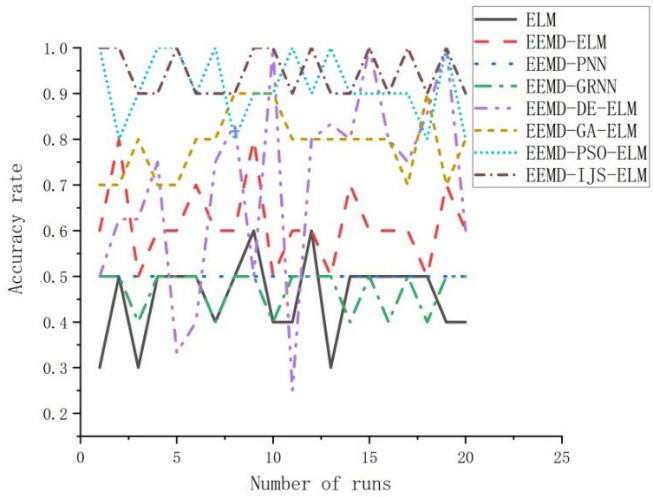


**Figure 16.** Statistics of accuracy of 20 tests of various models.

**Table 10.** Average statistics of recognition accuracy of various models in 20 tests.

| Fault diagnosis model | ELM | EEMD-ELM | EEMD-PNN | EEMD-GRNN | EEMD-DE-ELM | EEMD-GA-ELM | EEMD-PSO-ELM | EEMD-IJS-ELM |
|---|---|---|---|---|---|---|---|---|
| Accuracy rate | 45.5% | 61.5% | 50% | 47% | 70% | 79% | 91.5% | 95% |

According to Figure 16 and Table 10, we can know that the overall accuracy of ELM model is only 45.5%. The accuracy of EEMD-ELM has been significantly improved, and the overall accuracy reached 61.5%, but it was unstable and fluctuated between 50 and 80%. Although EEMD-PNN model and EEMD-GRNN model are stable, their accuracy is not as high as that of EEMD-ELM model. The overall accuracy is only 50 and 47% respectively, indicating that the accuracy of ELM is higher than that of ordinary neural networks. Although the accuracy of EEMD-DE-ELM model occasionally reaches 100%, its accuracy can reach 20% at the lowest, which is extremely unstable. The overall accuracy of EEMD-GA-ELM model is 79%. The average accuracy of EEMD-PSO-ELM of 20 times reaches 91.5%, the overall accuracy is above 90%.The accuracy of EEMD-IJS-ELM model is the highest, the average accuracy of 20 times reaches 95%, and the performance is the most stable. The accuracy rate only fluctuates between 90 and 100%.

To sum up, the accuracy and stability of EEMD-IJS-ELM industrial robot RV reducer fault diagnosis model are better than other 7 models.

## 6. Conclusions

RV reducer is one of the most important parts of robot. With the rapid development of robotics industry, RV reducer condition monitoring and fault diagnosis become particularly important. However, the traditional extreme learning machine network has the problem of low accuracy in performance evaluation of rotary vector reducer. To solve these problems, this paper proposes a fault diagnosis model of RV reducer based on EEMD-IJS-ELM. After comparative analysis, the following three conclusions are drawn:

1) The characteristic value of RV reducer in case of failure is decomposed by EEMD method based on the data measured on the RV reducer test platform, including potential characteristics of efficiency monitoring data. Through the introduction of tent mapping and competition mechanism, an improved artificial jellyfish search algorithm IJS algorithm is formed. After the standard function verification, the data show that the effect of IJS algorithm is better than JS algorithm, PSO algorithm and genetic algorithm. The model was substituted into XJTU-SY bearing experimental data set of Xi'an Jiaotong University, and the output results show that the accuracy of IJS-ELM fault diagnosis model is higher than that of JS-ELM fault diagnosis model and ELM fault diagnosis model.

2) Compared with the EEMD-IJS-ELM industrial robot RV reducer fault diagnosis and classification model constructed by this method and the ELM, EEMD-ELM, EEMD-PNN, EEMD-GRNN, EEMD-DE-ELM, EEMD-GA-ELM and EEMD-PSO-ELM models, The model is faster, more accurate and more stable. The reason why the new model can achieve a higher fault recognition rate is mainly because the IJS algorithm has strong global optimization characteristics, which can effectively overcome the inherent shortcomings of the random initialization of the traditional ELM initial weight. This method can also provide reference for other classifiers with

similar algorithms.

3) The proposed EEMD-IJS-ELM industrial robot RV reducer fault diagnosis classification model can timely and accurately judge the running state of the RV reducer, which is conducive to the timely maintenance of the RV reducer, can effectively help factories and enterprises to reduce losses, so as to achieve the purpose of improving the efficiency of the RV reducer manufacturers.

## Use of AI tools declaration

The authors declare they have not used Artificial Intelligence (AI) tools in the creation of this article.

## Acknowledgments

This research was funded by the Key Project of Scientific Research of Anhui Provincial Education Department, China, grant number No. 2022AH050995 and No. 2022AH050975; supported by Anhui Province Intelligent Mine Technology and Equipment Engineering Laboratory Open Fund, grant number No. AIMTEEL202201; Project of Science and Technology Bureau of Wuhu City, grant number No. KZ32022014; Open Fund of Anhui Key Laboratory of Electric Transmission and Control, grant number No. DQKJ202208; Research Project of Anhui Polytechnic University, grant number NO. Xjky2022007; Research Start-up Fund Project of Anhui Polytechnic University, grant number NO. 2022YQQ004; Applied Basic Research Project of Wuhu City, grant number NO. 2022jc20.

## Conflict of interest

The authors declare there is no conflict of interest.

## References

1. J. S. Shin, J. H. Kim, J. G. Kim, M. Jin, Development of a lifetime test bench for robot reducers for fault diagnosis and failure prognostics, *J. Drive Control*, **16** (2019), 33–41.
2. H. An, W. Liang, Y. Zhang, J. Tan, Hidden Markov model based rotate vector reducer fault detection using acoustic emissions, *Int. J. Sens. Netw.*, **32** (2020), 116–125. ttps://doi.org/10.1504/IJSNET.2020.104927
3. L. Chen, H. Hu, Z. Zhang, X. Wang, Application of nonlinear output frequency response functions and deep learning to RV reducer fault diagnosis, *IEEE Trans. Instrum. Meas.*, **70** (2020), 1–14. https://doi.org/10.1109/TIM.2020.3029383
4. A. Rohan, I. Raouf, H. S. Kim, Rotate vector (RV) reducer fault detection and diagnosis system: towards component level prognostics and health management (PHM), *Sensors*, **20** (2020), 6845. https://doi.org/10.3390/s20236845
5. S. Wang, J. Tan, J. Gu, D. Huang, Study on torsional vibration of RV reducer based on time-varying stiffness, *J. Vib. Eng. Technol.*, **9** (2021), 73–84. https://doi.org/10.1007/s42417-020-00211-8

6. I. Raouf, H. Lee, H. S. Kim, Mechanical fault detection based on machine learning for robotic RV reducer using electrical current signature analysis: a data-driven approach, *J. Comput. Des. Eng.*, **9** (2022), 417–433. https://doi.org/10.1093/jcde/qwac015
7. Q. Xu, C. Liu, E. Yang, M. Wang, An improved convolutional capsule network for compound fault diagnosis of RV reducers, *Sensors*, **22** (2022), 6442. https://doi.org/10.3390/s22176442
8. Y. He, H. Wang, S. Gu, New fault diagnosis approach for bearings based on parameter optimized VMD and genetic algorithm, *J. Vibr. Shock*, **40** (2021), 184–189. https://doi.org/10.13465/j.cnki.jvs.2021.06.025
9. Z. Huang, Y. C. Liu, R. J. Liao, X. J. Cao, Thermal error modeling of numerical control machine tools based on neural network neural network by optimized SSO algorithm, *J. Northeast. Univ. (Nat. Sci.)*, **42** (2021), 1569–1578. https://doi.org/10.12068/j.issn.1005-3026.2021.11.008
10. Z. Zhu, Y. Lei, G. Qi, Y. Chai, N. Mazur, Y. An, et al., A review of the application of deep learning in intelligent fault diagnosis of rotating machinery, *Measurement*, **206** (2022), 112346. https://doi.org/10.1016/j.measurement.2022.112346
11. X. Huang, G. Qi, N. Mazur, Y. Chai, Deep residual networks-based intelligent fault diagnosis method of planetary gearboxes in cloud environments, *Simul. Modell. Pract. Theory*, **116** (2022), 102469. https://doi.org/10.1016/j.simpat.2021.102469
12. F. He, Q. Ye, A bearing fault diagnosis method based on wavelet packet transform and convolutional neural network optimized by simulated annealing algorithm, *Sensors*, **22** (2022), 1410. https://doi.org/10.3390/s22041410
13. F. An, J. Wang, Rolling bearing fault diagnosis algorithm using overlapping group sparse-deep complex convolutional neural network, *Nonlinear Dyn.*, **108** (2022), 2353–2368. https://doi.org/10.1007/s11071-022-07314-9
14. K. Sharma, D. Goyal, R. Kanda, Intelligent fault diagnosis of bearings based on convolutional neural network using infrared thermography, *Proc. Inst. Mech. Eng., Part J: J. Eng. Tribol.*, **236** (2022), 2439–2446. https://doi.org/10.1177/13506501221082746
15. H. Wang, W. Jing, Y. Li, H. Yang, Fault diagnosis of fuel system based on improved extreme learning machine, *Neural Process. Lett.*, **53** (2021), 2553–2565. https://doi.org/10.1007/s11063-019-10186-7
16. B. H. Liu, M. M. Wang, Switch machine based on wavelet energy spectrum entropy and improved ELM fault prediction, *J. Yunnan Univ. (Nat. Sci. Ed.)*, **44** (2022), 497–504. https://doi.org/10.7540/j.ynu.20210174
17. X. L. Ge, X. Zhang, Bearing fault diagnosis method using singular energy spectrum and improved ELM, *J. Electr. Mach. Control*, **25** (2021), 80–87. https://doi.org/10.15938/j.emc.2021.05.010
18. V. K. Rayi, S. P. Mishra, J. Naik, P. K. Dash, Adaptive VMD based optimized deep learning mixed kernel ELM autoencoder for single and multistep wind power forecasting, *Energy*, **244** (2022), 122585. https://doi.org/10.1016/j.energy.2021.122585
19. J. S. Chou, D. N. Truong, A novel metaheuristic optimizer inspired by behavior of jellyfish in ocean, *Appl. Math. Comput.*, **389** (2021), 125535. https://doi.org/10.1016/j.amc.2020.125535
20. Z. Zhao, G. Ye, Y. Liu, Z. Zhang, Recognition of fault state of RV reducer based on self-organizing feature map neural network, *J. Phys. Conf. Ser.*, **1986** (2021), 012086. https://doi.org/10.1088/1742-6596/1986/1/012086

21. L. G. Kong, *Analysis Research in Reducer Fault Diagnosis Based on Fault Tree Method*, Master's thesis, Dalian University of Technology in Dalian, 2018.
22. J. F. Yu, S. Liu, F. F. Han, Z. Y. Xiao, Antlion optimization algorithm based on Cauchy variation (in Chinese), *Microelectron. Comput.*, **36** (2019), 45–49+54. https://doi.org/10.19304/j.cnki.issn1000-7180.2019.06.010
23. Y. B. Wang, *Research and Application of the Distance-Based Ant Lion Optimizer*, Master's thesis, Hunan University in Hunan, 2017.
24. R. C. Eberhart, Y. Shi, Comparing inertia weights and constriction factors in particle swarm optimization, in *Proceedings of the 2000 Congress on Evolutionary Computation*, **1** (2000), 84–88. https://doi.org/10.1109/CEC.2000.870279
25. Z. Wu, N. E. Huang, Ensemble empirical mode decomposition: a noise-assisted data analysis method, *Adv. Adapt. Data Anal.*, **1** (2009), 1–41. https://doi.org/10.1142/S1793536909000047
26. J. M. Chen, Z. C. Liang, Research on speech enhancement algorithm based on EEMD data preprocessing and DNN, *J. Ordnance Equip. Eng.*, **40** (2019), 96–103. https://doi.org/10.11809/bqzbgcxb2019.06.021
27. Y. J. Wang, S. Q. Kang, Y. Zhang, X. Liu, Y. C. Jiang, V. I. Mikulovich, Condition recognition method of rolling bearing based on ensemble empirical mode decomposition sensitive intrinsic mode function selection algorithm, *J. Electron. Inf. Technol.*, **36** (2014), 595–600. https://doi.org/10.3724/SP.J.1146.2013.00434
28. G. B. Huang, Q. Y. Zhu, C. K. Siew, Extreme learning machine: theory and applications, *Neurocomputing*, **70** (2006), 489–501. https://doi.org/10.1016/j.neucom.2005.12.126
29. B. Wang, Y. Lei, N. P. Li, N. B. Li, A hybrid prognostics approach for estimating remaining useful life of rolling element bearings, *IEEE Trans. Reliab.*, **69** (2018), 401–412. https://doi.org/10.1109/TR.2018.2882682
30. Y. G. Yang, *Research on Rolling Bearing Fault Diagnosis Method Based on Neural Network and Support Vector Machine*, Master's thesis, Lanzhou Jiaotong University in Lanzhou, 2021.



AIMS Press